Universidad de La Laguna

Stellar Evolution Models

P. Rosselló[1,*]

Assignment for the subject *Estructura y Evolución Estelar* of the master's degree in Astrophysics at Universidad de La Laguna (ULL).

1 Introduction

In this assignment we analyze the output of stellar models from [Ekström et al., 2012] for non-rotating stars with solar metallicities ($Z = 0.014$). The model output consists of one-dimensional time-series

$$S = \{S_i\}_{i=1}^{N} \tag{1}$$

for a given physical magnitude S of a star. N is the number of time-steps in the simulation, which changes from model to model; and S_i is the value of S at time-step i. The physical magnitudes we will be working with in the subsequent analysis are:

t	Age of the star.
X	Mass fraction of ^{1}He in the star's core.
Y	Mass fraction of ^{4}He in the core.
$Z^{(C)}$	Sum of the mass fractions of ^{12}C and ^{13}C in the core.
$Z^{(O)}$	Sum of the mass fractions of ^{16}O, ^{17}O, and ^{18}O in the core.
T_{eff}	Effective Temperature.
L	Luminosity.
T_c	Core Temperature.
ρ_c	Core Density.

Stellar model integration starts at the Zero-Age-Main-Sequence (ZAMS), so t_1 corresponds to the ZAMS. Also, it is worth mentioning that the time resolution $\Delta t_i \equiv t_i - t_{i-1}$ is not constant through the simulation, as it is determined by an adaptive time-step algorithm. The integration for the stellar models ends at the core helium flash for low mass stars, at the early Asymptotic Giant Branch (AGB) for medium mass stars, and at the end of the central carbon burning phase for high mass stars.

2 Results

2.1 Main Sequence of $5\,M_\odot$ and $9\,M_\odot$ Stars

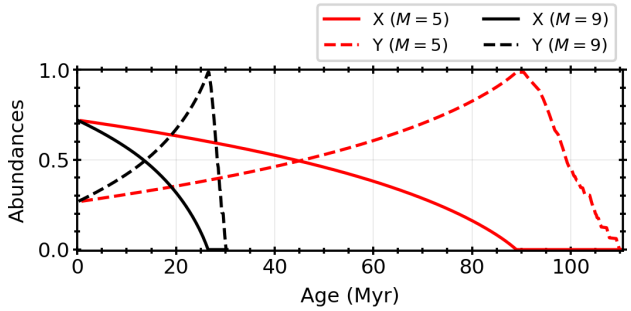

Figure 1: Abundances of H (solid line) and He (dashed line) over time for a $5\,M_\odot$ star (red) and a $9\,M_\odot$ star.

We start by looking at the abundances of Hydrogen, X and Helium, Y, for a $5\,M_\odot$ star and a $9\,M_\odot$ star. Results are represented in Figure 1. We see how X decreases significantly faster for $9\,M_\odot$ than for $5\,M_\odot$.

The H abundance allows us to define the MS lifetime of a star, τ_{MS}, as the time the star is steadily burning H in its core, with the MS ending with H core-exhaustion. For the stellar models we are working with, τ_{MS} can be defined as

$$\tau_{\text{MS}} = t_n - t_1 \ , \quad \text{where}$$
$$n = \min\{i \in \mathbb{N} \mid 1 \leq i \leq N \text{ and } X_i < \varepsilon\} \ . \tag{2}$$

for a given cutoff H exhaustion abundance, ε. That is, it is defined as the time it takes for the H abundance, X, to drop below ε. Choosing $\epsilon = 10^{-3}$ we find that $\tau_{\text{MS}} = 8.82 \times 10^6$ yr for a $5\,M_\odot$ star and $\tau_{\text{MS}} = 2.63 \times 10^6$ yr for a $9\,M_\odot$ star. The MS lifetime is shorter for the more massive star, which is in accordance with the H-burning rates observed in Figure 1. This result is expected as more massive stars have higher H-burning rates, due to the higher temperatures and pressures in their cores that allow for the CNO fusion cycle to take place. Low mass stars, on the other hand, burn H through the p–p chain reaction, which is less efficient and leads to longer MS lifetimes.

[1]Universidad de La Laguna
[*]alu0101693057@ull.edu.es

2.2 Hertzprung–Russell Diagram

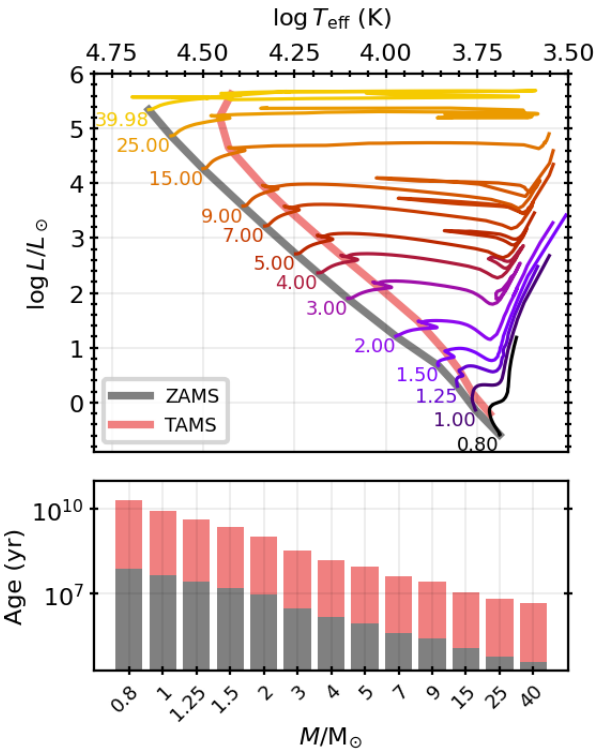

Figure 2: (Top) HR diagram showcasing stellar evolution tracks for stellar models with different masses. The grey line represents the ZAMS for all models. The pale-red line represents the TAMS for all models. Numbers represent the mass of the star in units of $M_\odot$. (Bottom) Values of the ZAMS (grey) and TAMS (pale-red).

Table 1: Values of the ZAMS and TAMS for models with different stellar masses.

Mass	ZAMS	TAMS
0.80	7.48×10^7	2.16×10^{10}
1.00	4.49×10^7	8.53×10^9
1.25	2.74×10^7	4.23×10^9
1.50	1.60×10^7	2.24×10^9
2.00	9.15×10^6	1.02×10^9
3.00	2.86×10^6	3.23×10^8
4.00	1.43×10^6	1.53×10^8
5.00	8.33×10^5	8.90×10^7
7.00	4.02×10^5	4.21×10^7
9.00	2.49×10^5	2.65×10^7
15.00	1.18×10^5	1.11×10^7
25.00	5.97×10^4	6.36×10^6
39.98	3.64×10^4	4.47×10^6

Stellar evolution tracks for different stellar masses are represented in Figure 2 (Top). The ZAMS and Terminal-Age-MS (TAMS) are represented in 2 (Bottom), with values in Table 1. The TAMS is defined as the time at which the star has exhausted all of its H in the core, thus TAMS $= t_n$ for all models, with n being the index defined in Eq. (2) for an H-exhaustion cutoff $\varepsilon = 10^{-3}$.

High mass stars have significantly shorter MS lifetimes than low stellar mass stars. The MS lifetime for the the $0.8\,M_\odot$ star model is 21.46 Gyr, while the MS lifetime for the $\sim 40\,M_\odot$ star is 4.44 Myr, more than 4 orders of magnitude shorter. The main reason is that high mass stars have higher core concentration and temperature which leads to more efficient nuclear reactions. This is reflected in the fact that the nuclear reaction rate is given by

$$q_{\rm nuc} \propto \rho T^n \ , \tag{3}$$

with n depending on the nuclear reaction, which in itself also depends on T. For the p–p chain, $n = 4$, while for the CNO cycle, $n = 16$.

2.3 Homology Relations

We now analyze the $\log L - \log M$, $\log T_c - \log M$ and $\log \rho_c - \log M$ relations for the stellar models at the ZAMS. We do so for stellar models of mass: 0.8, 1.0, 1.25, 1.5, 2.0, 3.0, 4.0, 5.0, 7.0, 9.0, 15.0, 25.0 and 39.98 $M_\odot$. Let us define

$$\alpha \equiv \frac{\log L}{\log M} \ , \tag{4}$$

$$\beta \equiv \frac{\log \rho_c}{\log M} \ , \tag{5}$$

$$\gamma \equiv \frac{\log T_c}{\log M} \ . \tag{6}$$

to be the slopes of the $\log L - \log M$, $\log T_c - \log M$ and $\log \rho_c - \log M$ relations respectively for the stellar models at the ZAMS. We compute each slope (α, β and γ) for sets of low, mid and high mass stars. The (rough) criteria for mass classification is as follows:

- **Low mass**: $0.35\,M_\odot < M < 2\,M_\odot$. Stars that burn H through the p–p chain reaction and are governed by a Kramers opacity law.
- **Mid mass**: $2\,M_\odot \leq M < 10\,M_\odot$. Stars that burn H through the CNO cycle and are governed by a Kramers opacity law.
- **High mass**: $M \geq 10\,M_\odot$. Stars that burn H through the CNO cycle and are governed by a

constant opacity coming from electron scattering.

These slopes are represented in Figure 3 for the different mass ranges of the stellar models. It is our goal now to compare these slopes with the slopes predicted by homology relations found in the literature for MS stars. The slopes found with homology relations are dependent on the mass ranges, as these are affected by the opacity law governing the star and its nuclear burning rate, which is different for the p–p chain and the CNO cycle. Finding the slopes through homology relations is rather cumbersome, and an outline of their derivation is included in Appendix A. For stars governed by a Kramers opacity law (low and mid mass stars), we find the following homology relations[1]:

$$\alpha = \frac{10n + 31}{5 + 2n} \tag{7}$$

$$\beta = \frac{2\,(n-3)\,(2n+11)}{(n+3)\,(2n+5)} \tag{8}$$

$$\gamma = \frac{-8n - 44}{(n+3)\,(2n+5)} \tag{9}$$

where n refers to the exponent of the temperature in the the nuclear burning rate equation $q_{\text{nuc}} \propto \rho T^n$, with $n = 4$ for the p–p chain (low mass) and $n = 16$ for the CNO cycle (mid mass). On the other hand, for stars governed by a constant opacity (high mass), we find:

$$\alpha = 3 \tag{10}$$

$$\beta = \frac{6 - 2n}{3 + n} \tag{11}$$

$$\gamma = \frac{4}{n+3} \tag{12}$$

where we always set $n = 16$ as high mass stars burn H through the CNO cycle.

The comparison between values found from the stellar model data and homology relations can be found in Table 2. We find that the slopes for the $\log L$–$\log M$ relation are in somewhat good agreement with the homology relations for all mass ranges, with the highest relative error being 0.297 for mid mass stars. The slopes for the $\log \rho_c$–$\log M$ found from the homology relations fail for low and high mass stars. We believe this is due to the rather wild assumption of associating the density of the star with the density in the core when deriving these relations (see footnote). Finally, the slopes for the $\log T_c$–$\log M$ relation are also in somewhat good agreement, with the highest deviation occurring for high mass stars (0.325 relative error). The relatively high relative errors between these relations are expected, as homology relations are derived from a series of assumptions that do not necessarily hold for the model stars, such as not considering convection and assuming a constant opacity law for the whole star.

Table 2: Slopes of the $\log L$–$\log M$ (α), $\log \rho_c$–$\log M$ (β) and $\log T_c$–$\log M$ (γ) relations for low, mid and high mass stars (see main text for mass classification criteria). Slopes are computed from model data and homology relations, and the relative error is included in the table. Model data is represented in Figure 3.

	Model Data	Hom. Rels.	Rel. Error
α_{low}	4.61	5.46	0.156
β_{low}	0.144	0.769	0.813
γ_{low}	0.727	0.923	0.212
α_{mid}	3.63	5.16	0.297
β_{mid}	−1.20	−1.03	−0.167
γ_{mid}	0.264	0.324	0.186
α_{high}	2.53	3.00	0.156
β_{high}	−0.805	−1.37	0.412
γ_{high}	0.142	0.211	0.325

[1] Homology relations for the density are found for the mean density of the star, which we assume to be representative of the density at the core, ρ_c.

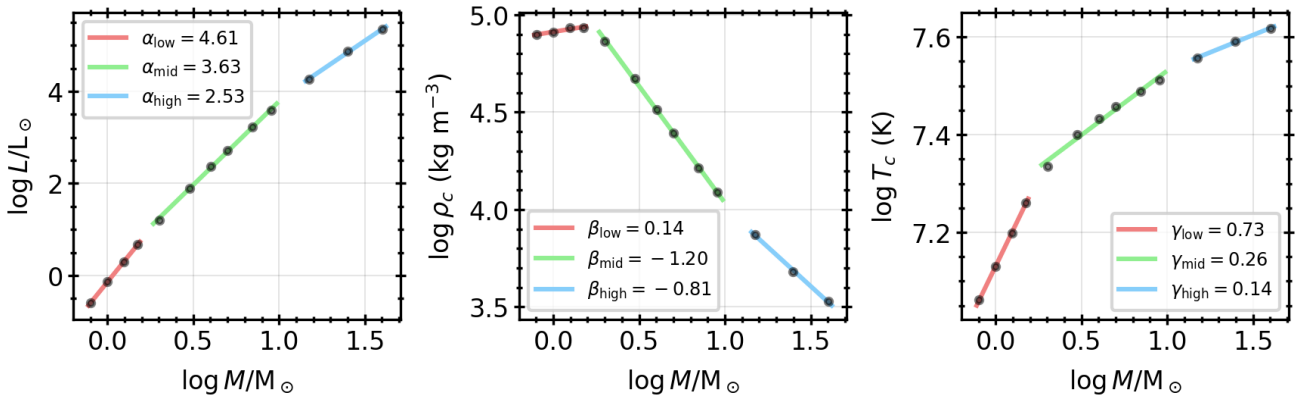

Figure 3: Slopes of the $\log L - \log M$ (α), $\log \rho_c - \log M$ (β) and $\log T_c - \log M$ (γ) relations for low, mid and high mass stars (see main text for mass classification criteria). In solar mass units, low mass stars are 0.8, 1.0, 1.25 and 1.5; mid mass stars are 2.0, 3.0, 4.0, 5.0, 7.0 and 8.0; and high mass stars are 14.0, 25.0 and 39.98.

2.4 The $\log T_c - \log \rho_c$ Plane

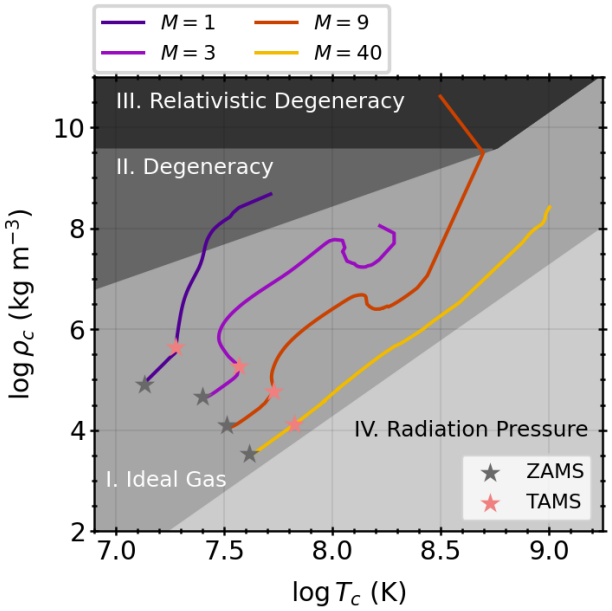

Figure 4: Stellar evolution tracks in the $\log T_c - \log \rho_c$ plane for stellar models with masses 1.0, 3.0, 9.0 and 40.0 $M_\odot$. The position of the ZAMS and the TAMS are marked with a pale-red and grey star respectively. The grey filling represents the domains where the star's core equation of state is governed by radiation pressure, the ideal gas law (for ions and electrons), electron degeneracy pressure, and relativistic electron degeneracy pressure.

Representing a star in the $\log T_c - \log \rho_c$ plane allows us to identify the equation of state governing the core of the star. The four regimes are

- **Clasical Ideal Gas Regime**: The equation of state for the ion and electron gas is

$$P_{\text{id}} = \frac{\mathcal{R}}{\mu} \rho_c T_c \tag{13}$$

  where $\mathcal{R} \equiv k_B/m_H = 8314\,\text{JK}^{-1}\text{kg}^{-1}$ is the gas constant and μ is the mean molecular weight ot the ions and electrons, which we set to 0.61.

- **Degenerate Electron Gas Regime**: The equation of state is

$$P_{\text{e-d}} = K_1 \rho_c^{5/3} \tag{14}$$

  where

$$K_1 = \left(\frac{3}{\pi}\right)^{\frac{2}{3}} \frac{h^2}{m_e (2m_H)^{5/3}}$$

- **Relativistic Electron Degeneracy Regime**: The equation of state is

$$P_{\text{e-rd}} = K_2 \rho_c^{4/3} \tag{15}$$

  where

$$K_2 = \left(\frac{3}{\pi}\right)^{\frac{1}{3}} \frac{hc}{8 (2m_H)^{4/3}}$$

- **Radiation Pressure Regime**: The equation of state is

$$P_{\text{rad}} = \frac{1}{3} a T_c^4 \tag{16}$$

  where

$$a = \frac{8\pi^5 k_B^4}{15 c^3 h^3}$$

By equating the different equations of state we can find the boundaries between the different regimes in the $\log T_c - \log \rho_c$ plane. These boundaries are represented in Figure 4 alongside the stellar evolution tracks for stellar models with masses 1.0, 3.0, 9.0 and 40.0 $M_\odot$. We observe that only the 1 $M_\odot$ star reaches electron degeneracy, while the 9 $M_\odot$ directly reaches relativistic electron degeneracy.

2.5 Analysis of a 4 $M_\odot$ star

We present now a thorough analysis of the evolution of the 4 $M_\odot$ stellar model. Relevant stellar magnitudes are represented in Figure 5. The –coarse-grained– phases of stellar evolution are:

- **Main Sequence (MS)** (A→B): The star steadily burns H in its core through the CNO cycle. Instead of defining the MS lifetime as the time it takes for the H abundance to drop below an insignificant H-exhaustion cutoff $\varepsilon = 10^{-3}$ (as done in Section 2.1), we set $\varepsilon = 0.03$. This way we differentiate the MS from the Hook (B→C) (see next bullet point). We find that the star is in its MS from 1.43 to 151.28 Myr, corresponding to a MS lifetime of 149.85 Myr. The nucleus contracts and heats up, as ρ_c and T_c steadily increase. L increases and T_{eff} decreases. The radius [2] R increases slowly from 2.15 to 4.69 $R_\odot$.
- **Hook** (B→C): Last stage of H burning as the star contracts in a Kelvin-Helmholtz timescale. R decreases from 4.69 to 4.16 $R_\odot$ with its consequent increase in T_{eff}, which creates a hook-like bend in the HR diagram. T_c and ρ_c increase proceeds. The star is in this phase from 151.28 to 153.44 Myr, lasting 2.61 Myr.
- **Hertzprung Gap (HG)** (C→D): Hydrogen has exhausted in the core and shell H burning pro-

[2] Not provided in the model data. It is computed using Stefan-Boltzmann Law: $L = 4\pi R^2 T_{\text{eff}}^4$.

ceeds. The core stars collapsing and the envelope of the star expands due to the mirror effect, with R increasing from 4.16 to 18.63 $R_\odot$. As core burning has stopped, and due to out-of-equilibrium processes, L decreases. We identify the end of this phase when L starts to increase again. The star is in this phase from 153.44 to 156.22 Myr, lasting 2.78 Myr.

- **Red Giant Branch (RGB)** (D→E): The core keeps contracting and heating up. R continues to increase rapidly from 18.63 to 50.74 $R_\odot$ as the star's envelope expands. As T_{eff} is roughly constant, L increases with R. This phase ends when the core has heated up enough to burn He. This is a short-lived phase: the star is in this phase from 156.22 to 156.94 Myr, lasting 0.72 Myr.
- **Blue Loop (BL)** (E→F): The core starts burning He. C and N abundances increase. It is a complex phase. The star performs a loop towards the blue region of the HR diagram and ends up in roughly the same place it started from. R decreases from 50.74 to 31.47 $R_\odot$. This phase ends when the core runs out of He. The star is in this phase from 156.94 to 194.48 Myr, lasting 37.54 Myr.
- **Asymptotic Giant Branch (AGB)** (F onwards): He burning stops. The core contracts and the envelope rapidly expands. R and L rapidly increase. The simulation run ends early in this phase, at 195.53 Myr age.

The radius R rapidly increases in two phases: during the HG+RGB and during the AGB. In both phases the core contracts and the envelope expands due to the mirror effect. In the HG+RGB the core contracts due to the exhaustion of H, and in the AGB the core contracts due to the exhaustion of He.

The model run ends early in the AGB phase. During this phase and onwards, stellar evolution theory tells us that as the star has exhausted H and He in its core, it burns these elements in shells surrounding a core mainly composed of C and O. The star would then begin a period of pulsations with recurrent surges in He burning and material being expelled from the outer layers of the star. A planetary nebulae forms. As the planetary nebulae disperses, the core of the star finally contracts and becomes a white dwarf.

3 Code Repository

The code used to produce the results in this assignment can be found at `https://github.com/pererossello/stellar_evolution_models`.
Two little bonus videos for the evolution of a $1\,M_\odot$ and $7\,M_\odot$ can be found in the `evolution_one_solar_mass.mp4` and `evolution_seven_solar_mass.mp4` files in the repository folder.

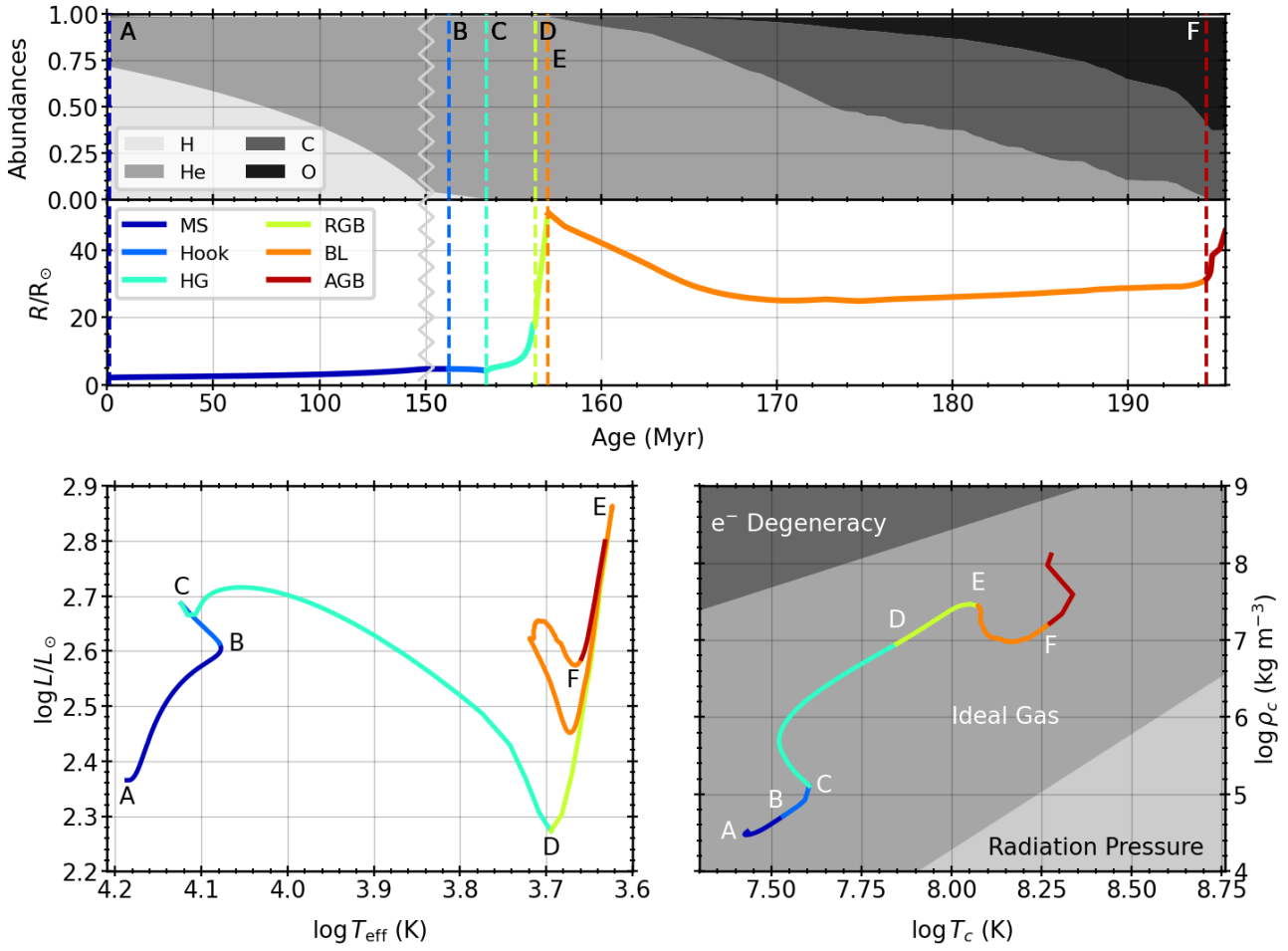

Figure 5: Evolution of a $4\,M_\odot$ star. Different phases of stellar evolution are depicted with letters and colors: Main Sequence (MS) in dark blue, A→B; Hook in light blue, B→C; Hertzprung Gap (HG) in cyan, C→D; Red Giant Branch (RGB) in yellow, D→E; Blue Loop (BL) in orange, E→F; and Asymptotic Giant Branch (AGB) in red, F onwards. (Top) Time series for abundances of H, He, C and O. (Middle) Time series for teh radius R. (Bottom-Left) Evolutionary track in the HR diagram. (Bottom-Right) Evolutionary track in the $\log T_c - \log \rho_c$ plane, with greyed filling indicating the equation of state regimes of the core.

References

Sylvia Ekström, Cyril Georgy, Patrick Eggenberger, Georges Meynet, Nami Mowlavi, Aurélien Wyttenbach, Anahí Granada, Thibaut Decressin, Raphael Hirschi, Urs Frischknecht, et al. Grids of stellar models with rotation-i. models from 0.8 to 120 m at solar metallicity (z= 0.014). *Astronomy & Astrophysics*, 537:A146, 2012.

Appendix

We present here an outline of the derivation of the homology relations. We assume the following relations to be our starting point:

$$L \propto M^3 \kappa \ , \tag{17}$$

$$T_c \propto M^{\frac{4}{n+3}} \kappa^{\frac{-1}{n+3}} \ , \tag{18}$$

$$\rho_c \propto M^{\frac{6-2n}{n+3}} \kappa^{\frac{-3}{n+3}} \ . \tag{19}$$

The opacity can be either

$$\kappa = \begin{cases} \kappa_{\text{Kr}} \propto \rho T^{\frac{-7}{2}} & \text{(Kramers)} \\ \kappa_{\text{es}} \equiv \text{cte} & (\text{e}^- \text{ scattering}) \end{cases} \tag{20}$$

If the opacity follows an electron scattering law, it is constant and it is trivial to see that from Eqs (17, 18, 19) we arrive at Eqs (10, 11, 12) in Sec. 3. If the opacity follows a Kramers law, we have to find an expression

$$\kappa_{\text{Kr}} \propto M^{\text{☹}} \ , \tag{21}$$

where ☹ is a function of n. That must be done by replacing ρ and T with adequate homology relations in a way that we are left only with dependence on M. We spare ourselves the pain of doing this here. After some algebraic juggling we arrive at

$$\kappa_{\text{Kr}} \propto M^{-\frac{4n+16}{5+2n}} \ . \tag{22}$$

Injecting this expression into Eqs (17, 18, 19) we arrive at Eqs (7, 8, 9) in Sec. 3.